Constraints on the viscosity of upper mantle and lower crust and the present-day surface deformation

Proposal: F 2

Jürgen Klotz, Christoph Reigber and Giorgi Khazaradze

Tectonic Setting of the Study Area

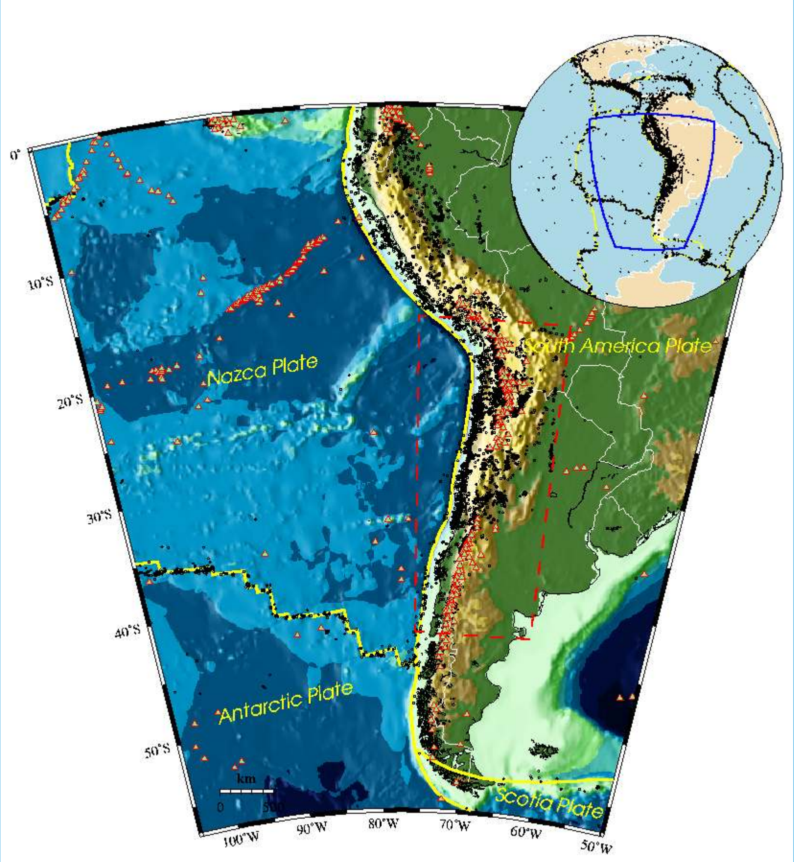

Black dots represent the distribution of seismicity from *Engdhal et al.*, [1998]; quaternary volcanoes are depicted as triangles [*Simkin and Siebert, 1994*]; Bathymetric and topographic data are based on *Smith and Sandwell* [1997].

Objective

One of the main factors controlling the evolution of the Andean orogen is the viscosity of the upper mantle and the lower crust. Constraints on the viscosity of the Earth at these depths can be derived from measurements of crustal deformation that are caused either by post-glacial rebound or post-seismic relaxation processes.

Main objective of our proposed work is to constrain the rheological properties of the upper mantle and the lower crust of the Earth. This will be achieved using our unique dataset of present-day crustal deformation measurements that includes post-seismic effects following the 1995 M_w8.0 Antofagasta and the 1960 M_w9.5 Valdivia earthquakes. Since our GPS measurements were conducted in very different time periods from the occurrence of the studied events, we hope to shed some light on time-dependence of post-seismic relaxation effect.

In addition, the results of our modeling will refine the estimate of the geometric extent of the seismic coupling between the subducting Nazca and the overriding South America plates. Also, our project will provide boundary conditions for the models of structural evolution of the Andean orogen developed by other groups within the SFB.

Earthquake Signals

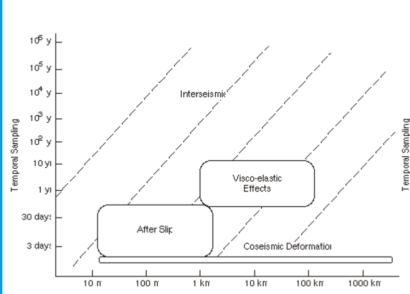

Temporal and spatial scales of Earth deformation related to earthquake processes. Figure from *Dixon* [1995].

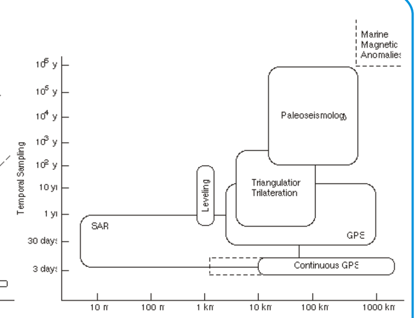

Temporal and spatial scales of various observation techniques relevant to earthquake studies. Figure from *Dixon* [1995].

Seismogenic Zone and Earthquake Cycle

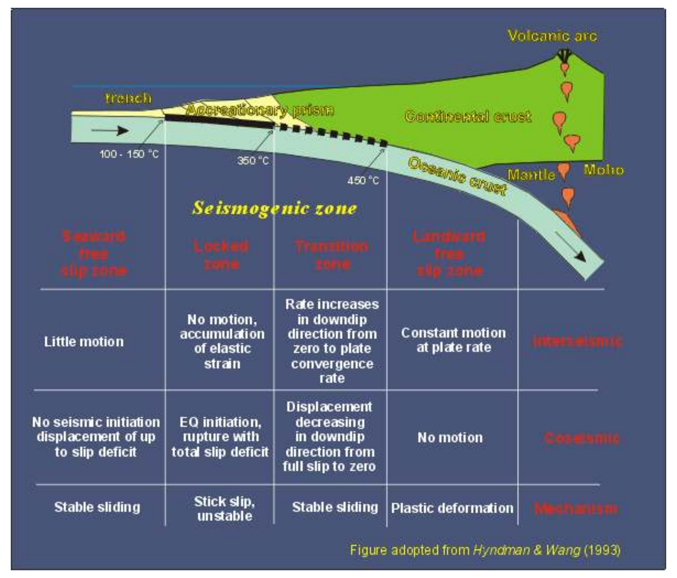

Schematic representation of subduction as used in an elastic dislocation model. The thrust fault is divided into *four* major zones. The main behavioral characteristics of each zone associated with different phases of earthquake cycle are summarized in the table. The figure is adopted from *Flück* (1997) based on *Hyndman and Wang* (1993).

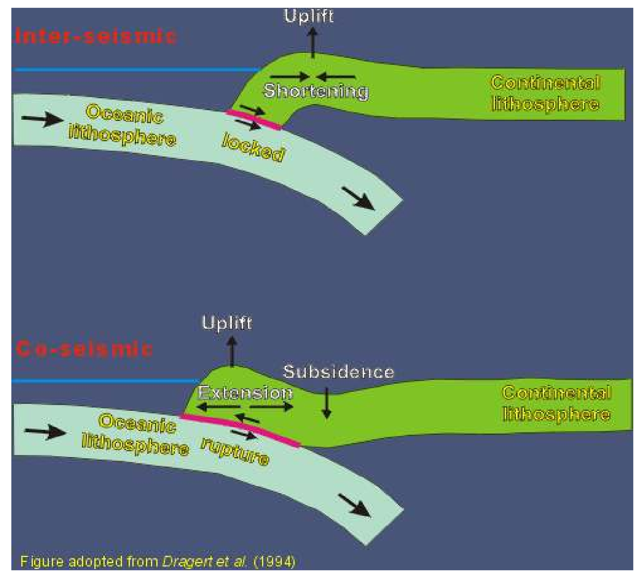

Schematic diagram illustrating the nature of expected surface deformations during the different phases of Earthquake cycle.

GPS Derived Velocity Field

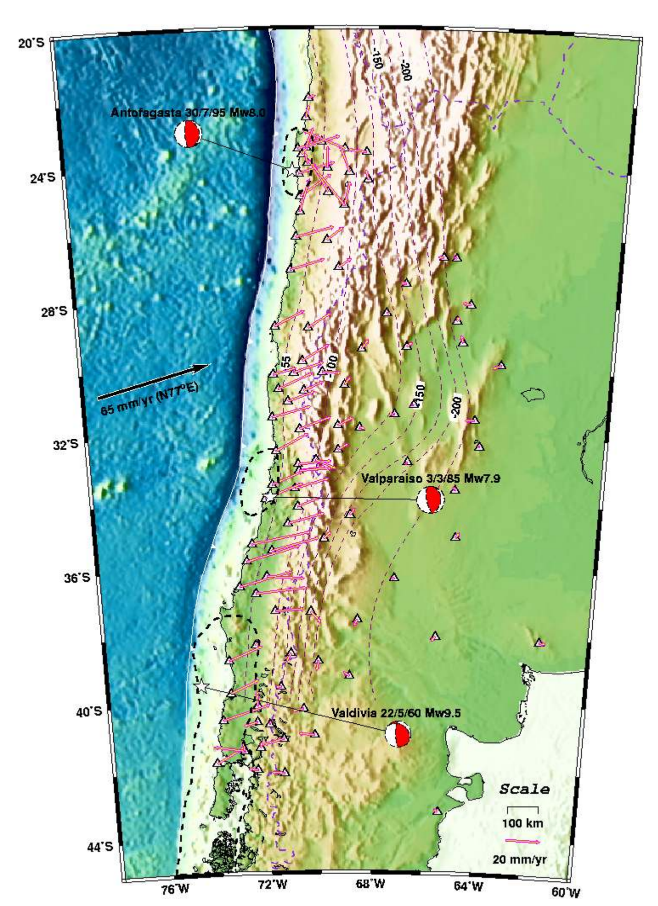

Velocity vectors based on 1994, 1995 and 1996 occupations. The epicenters, and the co-seismic rupture areas of 1995 M_w8.0 Antofagasta and 1960 M_w9.5 Chile earthquakes are shown with white stars and thick dashed lines, respectively. Nazca/South American plate convergence vector is based on the estimate of *Angermann et al.*, [1999].

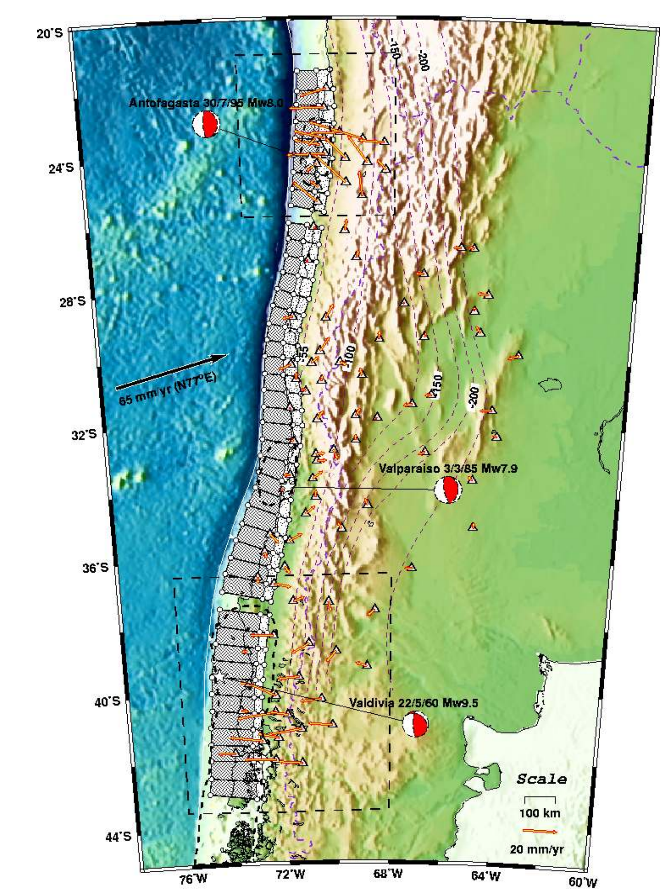

Seismogenic zone along the thrust interface deduced from the Andean Elastic Dislocation Model (AEDM). Vectors represent residual velocities obtained by subtracting the inter-seismic signal predicted by the AEDM from the observed velocities. Dashed contour lines represent the depth of the subducting Nazca slab estimated from Wadati-Benioff zone seismicity [*Cahill and Isacks, 1992; Cregaer et al., 1995*].

1960 M_w9.5 Valdivia Earthquake

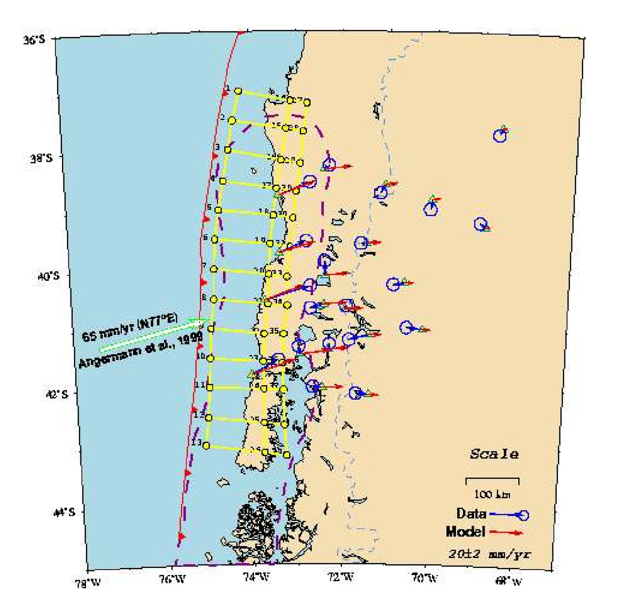

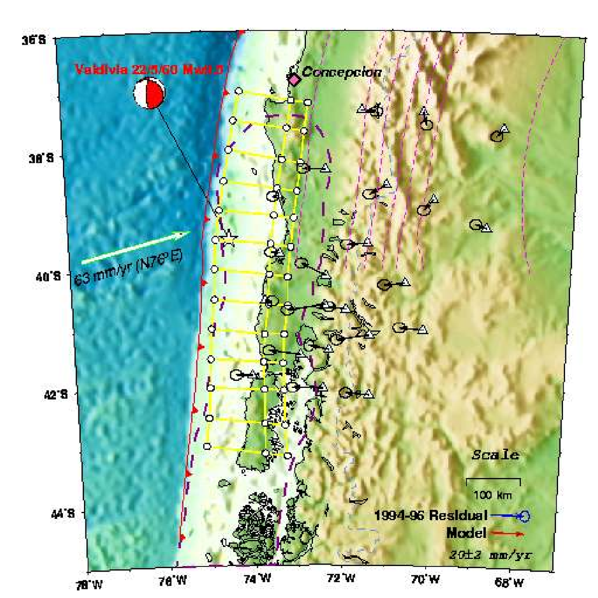

Post-seismic motions of the 1960 Valdivia earthquake are still clearly visible in the residual velocity field, 35 years after its occurrence. The residual velocity field was obtained by subtracting the AEDM predictions from the 1994-1996 observations.

1995 M_w8.0 Antofagasta Earthquake

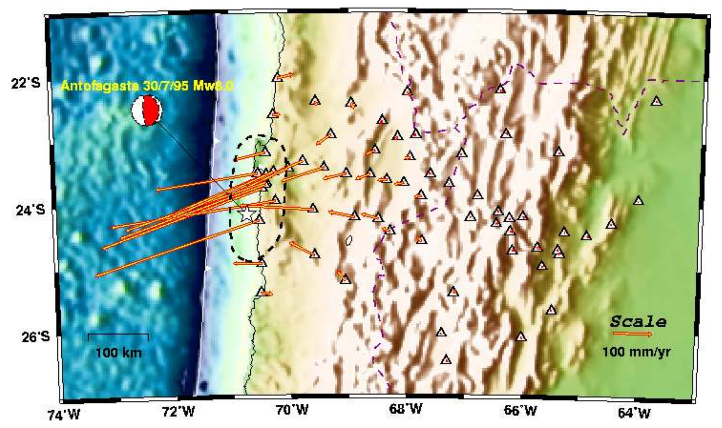

Co-seismic displacements during the M_w8.0 July 30th, 1995 Antofagasta earthquake [*Klotz et al., 1999*]. Measurements were conducted in 1993 and 1995, three months following the occurrence of the event.

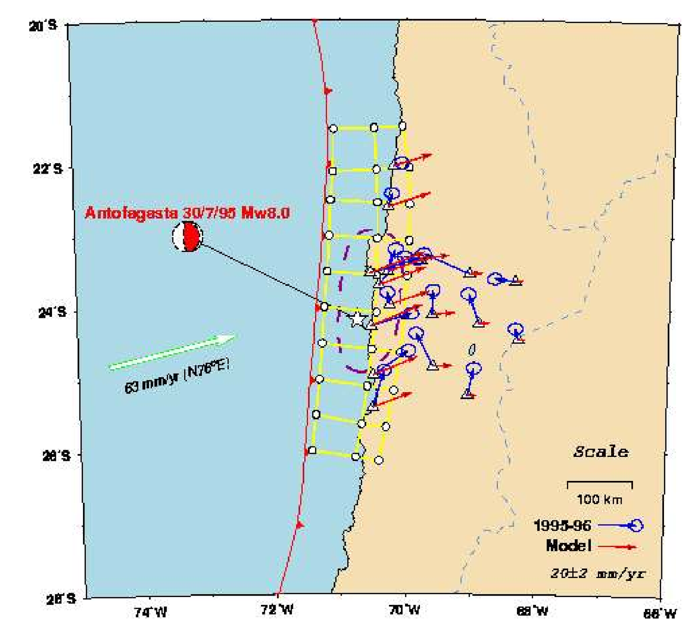

GPS Velocity field a year after the occurrence of the event (1995-1996) shown as blue vectors. The AEDM predicted velocities are shown in red. The grid with nodal points depicts the outline of the locked (seaward) and the transition (landward) zones.

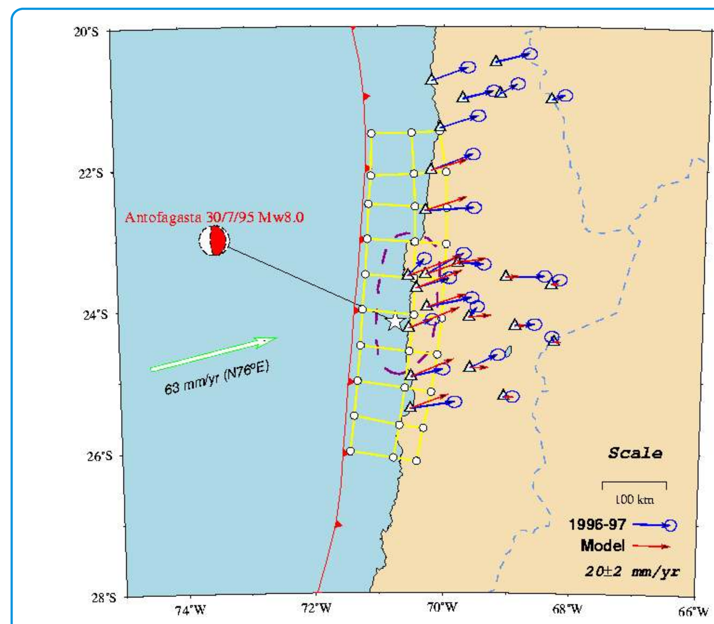

GPS Velocity field two years after the Antofagasta earthquake (1996-1997) shown as blue vectors. Note, that the AEDM (red vectors) explain the observations (blue vectors) considerably better than a year earlier (see the Figure above).

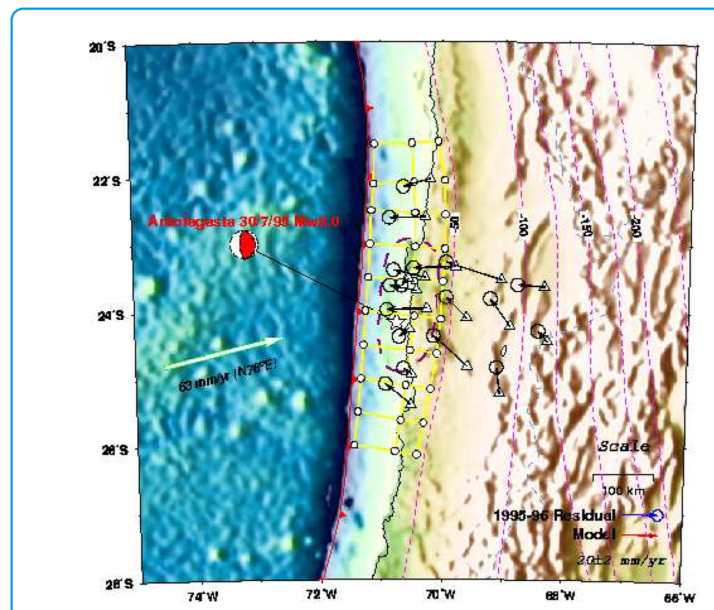

Post-seismic motions of the 1995 Antofagasta earthquake are clearly visible in the residual velocity field, one year after its occurrence. The residual velocity field was obtained by subtracting the AEDM predictions from the 1995-1996 observations.

Modeling Methods

Our main objective will be achieved with the aid of two independent modeling approaches: the first approach is based on an analytic formulation, which includes viscoelastic-gravitational layered Earth; the second approach will be based on numerical methods using a 3-D finite element model. The latter model is a further development of the 3-D elastic dislocation model which we used to explain present-day surface deformation in our previous work. The first model is relatively simple and has an analytic solution characterized with very high numerical accuracy (less than 1 % error) (*Fernandez and Rundle*, 1994). The second method, based on 3-D FEM approach, will enable us to represent the Earth much closer to its reality, including the complicated slab geometry and lithospheric and mantle stratification.

1st Method: Coupled viscoelastic-gravitational model (M1)

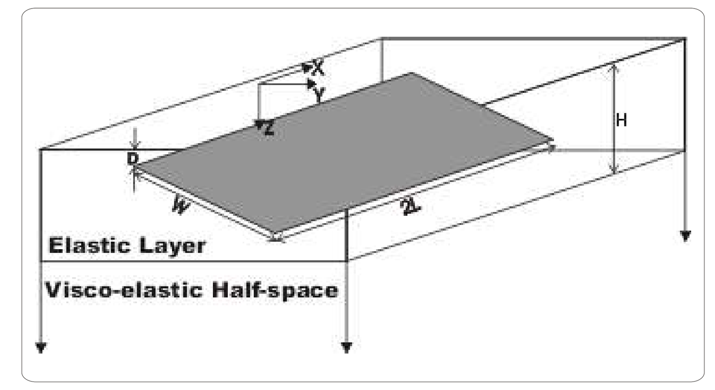

Earth Model: *one layer over homogenous half-space*

Layer:
- Properties: *elastic-gravitational*
- Parameters: *layer thickness, Lame parameters and density*

Half-space:
- Location: *viscoelastic-gravitational*
- Parameters: *Lame parameters, density and relaxation type*

Fault:
- Location: *layer*
- Parameters: *depth, fault plane width, length along Strike, dip angle*

Coordinate System:
- X axis: *parallel to the fault*
- Y Axis: *perpendicular to the fault*
- Z axis: *vertical positive down*
- Origin: *center of the fault*

Authors: *J. Fernandez, T. Ju and J. Rundle.*

2nd Method: Three-dimensional finite element model (M2)

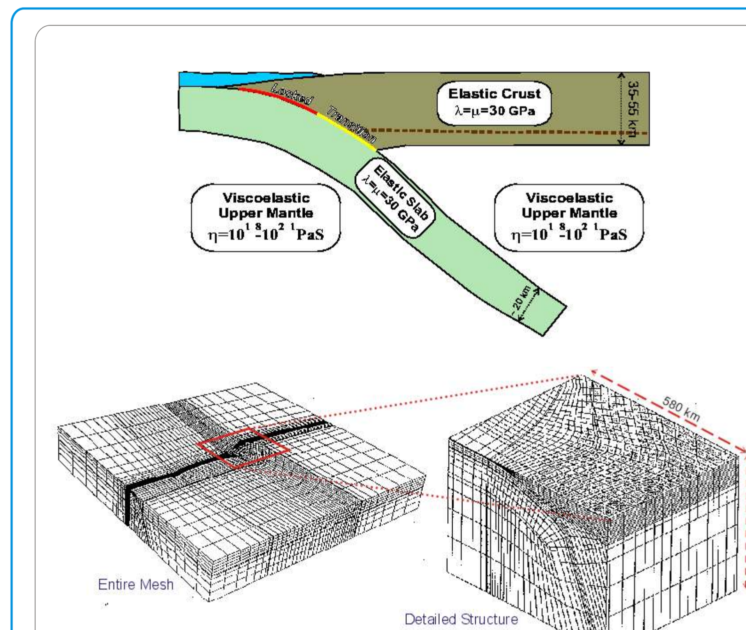

Earth Model: Defined by the finite element grid including the subducting oceanic plate

Code: Finite Element Program Generator developed by the Institute of Mathematics at the Chinese Academy of Sciences (*Liang*, 1991).

Authors: *K. Wang, J. He, H. Dragert and T. James*

Work Plan

1st year

In the first year of our project we will concentrate on modeling the observed post-seismic deformation rates using the 1st Method. Some of the initial parameters for this model are the same as used in our previous work with elastic dislocation models. However, unlike purely elastic models used in our previous work, the proposed viscoelastic models are characterized by the time-dependence. To detect the possibility of time dependent variations we intend to include in our modeling the time-series from continuous GPS stations located within the two study areas.

2nd year

In the second year of our project we will concentrate on modeling the observed pos-tseismic deformation rates using the second model by *Wang et al.*. Since the depth extent of the subducting slab in the 2nd model is far deeper (>400 km) than in the 1st model, it is important to constrain the precise geometry of the slab to this depth using various independent geophysical data. We will take into account the new findings regarding the structure of the crust along seismic refraction profiles. For the intermediate (50-100 km) depth ranges the geometry of the slab can be constrained using the locations of intra-slab earthquakes recorded at global and local seismic arrays (*Graeber and Asch*, 1999; *Husen et al.*, 1999), as well as from teleseismic receiver function studies (*Yuan et al.*, 2000). During the second half of the 2nd year we intend to switch towards the more complicated models, where the crust will include the lower layer with a viscoelastic rheology and the underlying mantle will consist of several viscoelastic layers characterized by changing rheological properties.

3rd year

In the third year of our proposed research we will perform a comprehensive comparison of the results from our two independent modeling approaches. At this stage other subprojects within the SFB will also have important new results and we will concentrate on a joint interpretation including publications.

References

Angermann, D., J. Klotz, and C. Reigber, Space-geodetic estimation of the Nazca-South America Euler vector, *Earth Planet. Sci. Lett.*, *171* (3), 329-334, 1999.

Cahill, T., and B.L. Isacks, Seismicity and shape of the subducted Nazca Plate, *J. Geophys. Res.*, *97* (12), 17503-17529, 1992.

Creager, K.C., C. Ling Yun, J.P. Winchester, and E.R. Engdahl, Membrane strain rates in the subducting plate beneath South America, *Geophys. Res. Lett.*, *22* (16), 2321-2324, 1995.

Dixon, T.H., SAR interferometry and surface change detection, pp. 97, RSMAS, Univ. of Maiami, Miami, USA, 1995.

Dragert, H., R.D. Hyndman, G.C. Rogers, and K. Wang, Current deformation and the width of the seismogenic zone of the northern Cascadia subduction thrust, *J. Geophys. Res.*, *99* (B1), 653-668, 1994.

Engdahl, E.R., R. Van der Hilst, and R. Buland, Global teleseismic earthquake relocation with improved travel times and procedures for depth determination, *Bull. Seismol. Soc. Amer.*, *88* (3), 722-743, 1998.

Fernandez, J., and J.B. Rundle, Gravity changes and deformation due to a magmatic intrusion in a two-layered crustal model, *J. Geophys. Res.*, *99* (2), 2737-2746, 1994.

Fernandez, J., T.T. Yu, and J.B. Rundle, Deformation produced by a rectangular dipping fault in a viscoelastic-gravitational layered Earth model; Part I, Thrust fault; FLTGREV and FLTGRH Fortran programs, *Computers & Geosciences*, *22* (7), 735-750, 1996a.

Fernandez, J., T.T. Yu, and J.B. Rundle, Horizontal viscoelastic-gravitational displacement due to a rectangular dipping thrust fault in a layered Earth model, *J. Geophys. Res.*, *101* (6), 13,581-513,594, 1996b.

Flück, P., R.D. Hyndman, and K. Wang, Three-dimensional dislocation model for great earthquakes of the Cascadia subduction zone, *J. Geophys. Res.*, *102* (9), 20539-20550, 1997.

Graeber, F., and G. Asch, Three dimensional models of P-wave velocity and P-to-S velocity ratio in the southern central Andes by simultaneous inversion of local earthquake data, *J. Geophys. Res.*, *104* (9), 20,237-220,256, 1999.

Husen, S., E. Kissling, E. Flueh, and G. Asch, Accurate hypocentre determination in the seismogenic zone of the subducting Nazca Plate in northern Chile using a combined on-/ offshore network, *Geophys. J. Int.*, *138* (3), 687-701, 1999.

Hyndman, R.D., and K. Wang, Thermal constraints on the zone of major thrust earthquake failure; the Cascadia subduction zone, *J. Geophys. Res.*, *98* (2), 2039-2060, 1993.

Klotz, J., D. Angermann, G.W. Michel, R. Porth, C. Reigber, J. Reinking, J. Viramonte, R. Perdomo, V.H. Rios, S. Barrientos, R. Barriga, and O. Cifuentes, GPS-derived deformation of the Central Andes including the 1995 Antofagasta M (sub w) = 8.0 earthquake, *Pure Appl. Geophys.*, *154*, 3709-3730, 1999.

Smith, W.H.F., and D.T. Sandwell, Global sea floor topography from satellite altimetry and ship depth soundings, *Science*, *277* (5334), 1956-1962, 1997.

Wang, K., J. He, H. Dragert, and T. James, Three-dimensional viscoelastic interseismic deformation model for the Cascadia subduction zone, *Earth Planet Space*, *53*, 295-306, 2001.

Yu, T.T., J.B. Rundle, and J. Fernandez, Deformation produced by a rectangular dipping fault in a viscoelastic-gravitational layered Earth model; Part II, Strike-slip fault; STRGRV and STRGRH Fortran programs, *Computers & Geosciences*, *22* (7), 751-764, 1996.